Studying the Effect of Stiffener Configurations on the Structural Response of Hopper Wagon Using Finite Element Analysis

Rafif Ibnu Ardiansyah, Achmad Fauzan Hery Soegiharto*, Mohamad Irkham Mamungkas, Abi Mufid Octavio

Department of Mechanical Engineering, University of Muhammadiyah Malang, Malang, Indonesia

Received 25 March 2026; revised 08 May 2026; accepted 14 May 2026

DOI: https://doi.org/10.46604/aiti.2026.16309

Abstract

Hopper wagons are subjected to complex loading conditions during granular material transportation. This study aims to evaluate the effect of stiffener configurations on the structural response of a hopper wagon using finite-element analysis under multi-compartment loading conditions. Three configurations are analyzed: vertical, rectangular, and triangulated stiffeners, with a non-uniform distribution of granular material to reflect real-world operating conditions. The results show that the triangulated configuration exhibits the lowest average deformation (15.466 mm) and a more uniform stress distribution. The vertical configuration yields the lowest maximum stress and the highest safety factor, but is less effective at controlling global deformation. Conversely, the rectangular configuration increases structural stiffness but produces stresses close to the material's yield limit. The analysis also indicates that the most critical loading conditions do not always occur under full loading. Overall, the triangulated configuration provides the best balance among stiffness, stability, and structural safety across various loading conditions.

Keywords: hopper wagon, stiffener configuration, finite element analysis, multi-compartment loading, structural response

1. Introduction

The transportation of bulk materials remains one of the primary functions in rail-based logistics systems. Various commodities, such as ballast, construction materials, sand, and coal, are typically transported using hopper cars. These cars enable rapid loading and unloading through a gravity-fed mechanism at the bottom of the car. In operational practice, hopper cars play a vital role in large-scale material distribution chains, particularly in the mining and construction industries [1]. While the system is relatively simple operationally, it is structurally more complex than it appears from a structural standpoint [2]. The hopper must withstand the weight of large volumes of material while also accommodating fluctuating loads during train transit [3]. The combination of material pressure and vehicle operational conditions means that the structural design of the hopper cannot be treated as a purely static problem.

The material inside the hopper does not merely impose a vertical load due to its weight [4]. Granular particles also transfer lateral pressure to the hopper walls through particle-particle interactions and friction with the plate surface [5]. Consequently, the hopper plates experience a complex two-way stress state [6]. During operation, these conditions are influenced by vehicle vibrations and wheel-rail interactions [7]. However, in many studies of rail vehicle structures, dynamic effects are often first represented using an equivalent static loading approach [8]. This approach is commonly used when the analysis focuses on stress distribution resulting from material pressure and structural plate configurations [9].

* Corresponding author. E-mail address: achmadfauzan@umm.ac.id

In actual operation, the loading process rarely produces a perfectly uniform load distribution [10]. Material is typically poured gradually, so some hopper compartments may fill up before others [11]. This condition causes the force distribution on the hopper structure to become asymmetric [12]. The hopper wall plates then experience increased local bending in certain areas [13]. In freight car maintenance inspection reports, these areas often represent the initial locations where structure deformation or cracks appear [14].

Several previous studies have attempted to understand the structural behavior of freight railcars using various approaches. Numerical methods based on finite element analysis are widely used to evaluate stress distribution in the railcar body, as demonstrated by Lv [15]. Through this approach, the structural response under various loading conditions can be analyzed in greater detail. Some studies have focused on the wagon's main frame or bogie system to examine how dynamic loads affect the vehicle's structural integrity, including the work of Xiao et al. [16].

Research on granular material inside the hopper has also received considerable attention [17]. Classical models such as Rankine's or Janssen's theories are often used to estimate bulk pressure against the wagon hopper walls, as reviewed by Dyck et al. [18]. These models indicate that granular pressure does not always follow a hydrostatic distribution. Some studies have even attempted to model this phenomenon using numerical approaches to obtain more realistic pressure distributions, such as that proposed by Eidin et al. [19]. Additionally, many hopper studies often treat the hopper as a mere material container, without a deeper discussion of the structural behavior of its plates, as discussed by Vatulia et al. [20].

When considering the literature as a whole, it is evident that research focus remains largely directed toward two areas. The first is the global strength analysis of the wagon structure. The second is the behavior of granular material inside the hopper. Meanwhile, discussions of how the plate stiffener configuration affects the hopper's structural response have received comparatively less attention. The hopper plate is essentially a thin plate structure reinforced by stiffeners. In such structures, the stiffener pattern plays a crucial role in determining the path of force distribution.

Another limitation of previous research relates to the loading assumptions used. Many studies assume a uniform load distribution throughout the hopper volume, as reported by Panchenko et al. [21]. In operational practice, such conditions rarely occur. Material is often distributed unevenly due to the gradual loading process. This imbalance in load distribution can result in more severe loading conditions than those predicted under uniform loading assumptions, as highlighted by Sookchanchai et al. [22]. Furthermore, most studies evaluate only a single structural configuration without providing systematic comparisons across other configurations that may yield different responses.

This situation indicates that there remains a significant research gap in this area. Specifically, the relationship between stiffener configurations and stress distribution in the hopper plate has not yet been comprehensively investigated. Research examining various stiffener configurations comparatively is also still relatively limited. This is particularly true for hopper wagons used to transport heavy granular materials such as railway ballast.

Given these conditions, this study aims to evaluate the influence of stiffener configurations on the structural behavior of hopper wagons. The analysis is conducted by considering several variations in stiffener configurations on the hopper plate. Additionally, the load distribution within the hopper is not assumed to be uniform. Several loading scenarios were used to represent various possible conditions of hopper compartment filling. This approach is expected to provide a more realistic representation of how the hopper structure responds to different force distributions.

The main contribution of this study lies in the comparative approach to stiffener configurations on the hopper plate. Several stiffener patterns were analyzed, including vertical, rectangular, and triangulated stiffener configurations. By comparing the structural response of each configuration, this study identifies the most effective stiffener pattern for enhancing structural stiffness and reducing stress concentrations. Furthermore, the use of various load distribution scenarios allows for a

more representative evaluation of the operational conditions of hopper wagons. The results of this study provide a clearer understanding of the relationship between stiffener configurations and the structural performance of hoppers, as well as serve as a basis for developing more reliable hopper wagon designs.

2. Materials and Methods

This study was conducted using a finite element methodology to evaluate the structural response of hopper wagon walls under granular loading conditions. The analysis focused on how different stiffener configurations affect deformation, strain, and stress. The numerical model incorporated material properties, hopper geometry, stiffener arrangement, loading conditions, and mesh generation. All configurations were analyzed under identical conditions to ensure a consistent comparison.

2.1 Material properties

The material used in this study is 09G2S structural steel [23]. This material is a low-alloy steel commonly used in railways and structures operating under heavy loads. It was selected because it offers a good combination of strength and toughness with good resistance to fracture under demanding service conditions. In railway applications, this material is also known for its good resistance to cyclic loading.

In the numerical simulations of this study, the material is assumed to be linearly elastic and isotropic. This assumption is used to represent the material's elastic behavior during the initial stage of deformation, where stresses remain below the material's yield point. The relationship between stress and strain still follows Hooke's law. Thus, the structural response can be analyzed using the material's basic elastic properties. The material property data are provided in Table 1.

Table 1 Properties of 09G2S structural steel

Property	Symbol	Value	Unit
Density	ρ	7.85×10^3	kg/m³
Young's Modulus	E	2.10×10^5	MPa
Poisson's Ratio	ν	0.30	-
Bulk Modulus	K	1.75×10^5	MPa
Shear Modulus	G	8.08×10^4	MPa
Tensile Yield Strength	σ_γ	3.55×10^2	MPa
Tensile Ultimate Strength	σ_u	5.10×10^2	MPa

2.2 Geometry model and stiffener configuration

The geometry of the hopper car used in this study was developed based on the typical configuration of railway cars. This type of hopper car is designed to transport granular materials such as rail ballast, construction aggregates, or mining materials. The main structure consists of side plate walls, internal partitions, and an inverted cone-shaped hopper section. This cone directs the material toward the unloading mechanism at the bottom.

The hopper model used has a total length of approximately 10 m, a width of approximately 3 m, and a structural height of approximately 2.6 m. The hopper structure is divided into four main compartments separated by internal partitions. This compartmentalization not only serves as a material distribution barrier but also as a structural element that helps transfer forces to the wagon's main frame. This geometry was then used as the basis for developing the structural model in numerical simulations. The geometry, dimensions, and example of the hopper wagon are shown in Figs. 1 and 2.

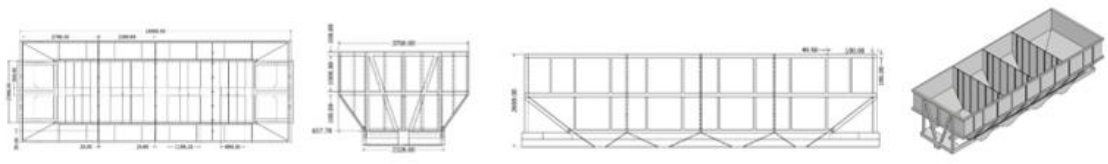

Fig. 1 Geometry and dimensions of hopper wagon in mm

Fig. 2 Example of hopper wagon

After the basic geometric model is established, plate stiffeners are added to the hopper walls. The addition of stiffeners aims to enhance the structural stiffness of the plates and reduce deformation caused by granular material pressure [24]. In thin-plate structures such as hopper walls, lateral pressure from the material can cause significant local bending. The first configuration is the vertical stiffener configuration, in which stiffeners are installed vertically along the hopper plate. The second configuration is the rectangular stiffener configuration, which forms a grid pattern through a combination of vertical and horizontal stiffeners. The third configuration is the triangulated stiffener configuration, which uses a triangulation pattern to increase structural stiffness through a triangular frame mechanism. These three configurations are shown in Fig. 3.

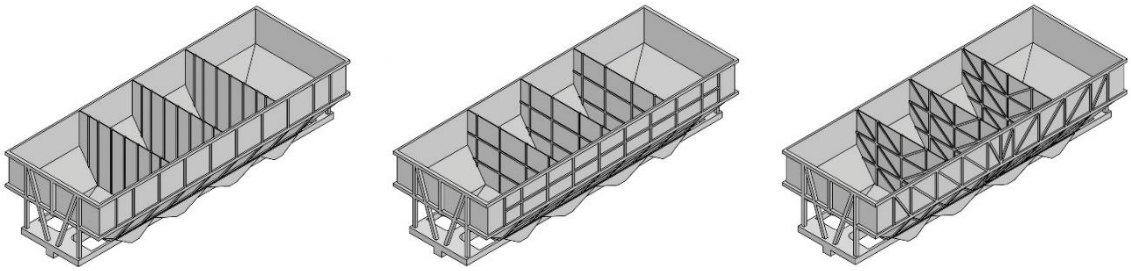

(a) Vertical stiffener (b) Rectangular stiffener (c) Triangulated Stiffener

Fig. 3 Stiffener design configurations for hopper wagons

The stiffener arrangements were selected to represent different reinforcement approaches commonly found in hopper structures. Their spacing was adjusted according to the hopper wall dimensions to maintain comparable structural proportions. The selected layouts were intended to provide representative structural behavior under the same loading conditions.

Nine vertical stiffeners were used in the longitudinal configuration. A denser arrangement could further increase stiffness and reduce wall deformation. However, additional stiffeners would also increase plate intersections, welding work, and structural weight. Similar considerations were applied to the rectangular configuration. Using a smaller grid spacing would likely improve local rigidity, although fabrication complexity and production cost would also increase.

The triangulated configuration did not include diagonal members in every panel region. Partial triangulation was adopted to avoid excessive reinforcement density in several hopper sections. This arrangement was considered sufficient to alter the force transfer mechanism without significantly increasing fabrication difficulty. Different stiffener quantities or spacings may lead to different deformation and stress responses. Therefore, the present study is limited to the assumed stiffener geometries defined in the numerical model.

2.3 Finite element modeling

The finite element model was developed to evaluate the structural response of the hopper wagon across different stiffener configurations and loading combinations. The simulation includes defining boundary conditions, calculating pressure loads, modeling multi-compartment loading scenarios, and generating the mesh. All configurations were analyzed using identical material properties, loading conditions, and support constraints to ensure a consistent comparative framework. The modeling procedure was designed to capture the deformation, strain, and stress distributions of the hopper structure under granular loading conditions.

2.3.1 Boundary conditions

The boundary conditions in the model consist of a fixed support applied at the lower frame of the hopper, which is connected to the bogie system. The fixed support area is shown in Fig. 4. This area serves as the primary load transfer point between the wagon body and the train wheel system. In the numerical model, the support is constrained in all degrees of freedom for both translation and rotation, and is therefore modeled as a fully fixed boundary condition. This approach is used to represent the structural condition of the hopper, which is supported by the wagon's main frame during operation.

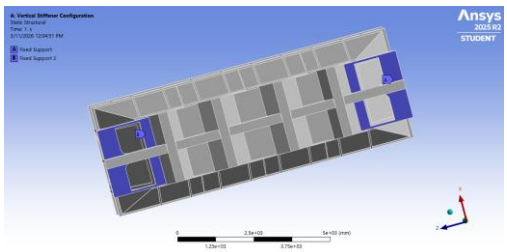

Fig. 4 Fixed support in a static structural simulation

2.3.2 Pressure loading

The pressure exerted on the hopper walls by the crushed stone was calculated using the material bulk density, gravitational acceleration, material height, and internal friction angle [25]. In this study, the applied pressure represents an equivalent static lateral pressure acting normal to the hopper wall surfaces. For simplicity in the static structural simulation, the pressure was assumed to be uniformly distributed over each wall panel. The lateral pressure acting on the hopper wall is expressed as:

$$p_a = \gamma g H \tan^2(45° - \frac{\varphi}{2}) \tag{1}$$

where P is the lateral pressure acting normal to the hopper wall surface (MPa), γ is the bulk density of the material (t/m³), g is the gravitational acceleration (9.81 m/s²), h is the material height inside the hopper (m), and φ is the internal friction angle of the granular material.

The pressure magnitude varies depending on the inclination angle of the hopper wall. Because the normal component of the granular force changes with wall orientation. Hopper walls with steeper inclinations experience higher normal pressure compared to more inclined wall sections.

The ballast material density used in this study was 1.50 t/m³ with a material height of 2.4 m. Based on the calculation, the maximum lateral pressure acting on the vertical wall section (90° inclination) was 0.00657 MPa. Using the same calculation approach, the pressures acting on hopper wall inclinations of 54°, 38°, and 24° were determined as 0.00447 MPa, 0.00296 MPa, and 0.00164 MPa, respectively. These pressure values were subsequently applied as uniformly distributed loads normal to the corresponding hopper wall surfaces in the finite element model. Thus, each wall section received a pressure magnitude according to its geometric inclination angle.

2.3.3 Multi-compartment loading

The loading scheme was designed to represent the distribution of granular material during operation. The hopper model consists of four main compartments separated by internal partitions. Granular material pressure was applied to the hopper plate surface in a direction perpendicular to the plate surface [26]. The presence of partitions in the hopper operates on a mechanical principle similar to that of baffles in fluid tanks. Although granular material does not behave exactly like a fluid, particle redistribution may still occur due to vibrations, acceleration changes, or the path inclination [27]. The hopper is divided into four loading sections by three internal partitions, which help restrict material movement while channeling pressure toward the wagon's main frame, as shown in Fig. 5.

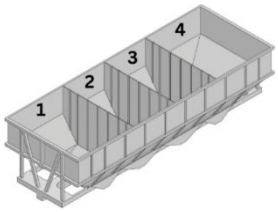

Fig. 5 Sections of hopper wagon

To evaluate the effect of load distribution, several compartment loading combinations were modeled in the simulation. These combinations include 1, 1-2, 1-2-3, and 1-2-3-4 as presented in Fig. 6. These variations allow for analysis of both symmetric and asymmetric loading conditions. Thus, the structural response of the hopper can be observed under various material distribution conditions, enabling critical stress concentrations to be identified more accurately.

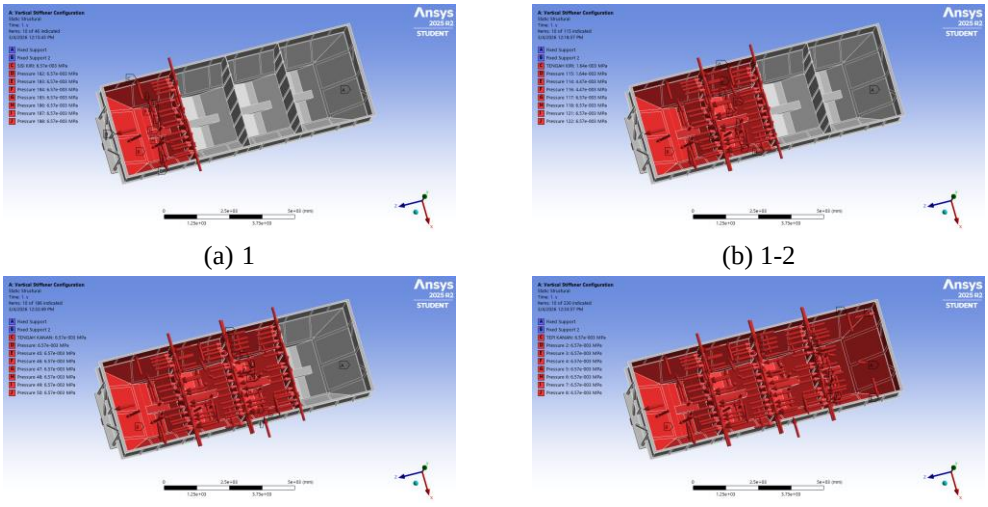

(a) 1 (b) 1-2

(c) 1-2-3 (d) 1-2-3-4

Fig. 6 Critical loading combinations

2.3.4 Mesh generation

The geometric model of the hopper wagon was discretized using a meshing process to convert the continuous geometry into numerical elements. The mesh consists predominantly of quadrilaterals on the surface of the structure. This mesh type (quadrilateral–dominant) was chosen because the hopper's geometry consists largely of plate structures. Furthermore, these mesh elements are generally more suitable for representing the stress distribution in the plates more accurately than tetrahedral elements. The mesh visualization and its specifications are shown in Fig. 7 and Table 2.

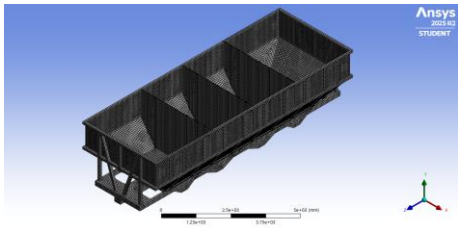

Fig. 7 Mesh generation

Table 2 Specification of mesh

Parameter	Value	Unit
Element Size	60	mm
Number of Elements	76,237	-
Number of Nodes	75,868	-
Bounding Box Diagonal	11,123	mm
Average Surface Area	3.5509×10^5	-
Minimum Edge Length	1.0383	mm
Maximum Layers	5	-
Growth Rate	1.2	-

3. Results

The finite element simulations were performed to evaluate the structural response of the hopper wagon. Different stiffener configurations and loading combinations were analyzed in the simulations. The structural response was evaluated based on total deformation, equivalent elastic strain, and equivalent (von-Mises) stress. Each configuration was analyzed under the same loading conditions to ensure a consistent basis for comparison. The results were then compared to identify the influence of stiffener topology on structural behavior.

3.1 Structural response of vertical stiffener configuration

The simulation results for the vertical stiffener are shown in Figs. 8-10 and Table 3. The results indicate that the vertical stiffener is capable of maintaining stress levels within a relatively moderate range. However, this configuration shows limited effectiveness in controlling the global deformation of the hopper plate. In this configuration, the stiffener acts predominantly in the height direction of the plate. The transfer of granular pressure forces tends to be directed along the vertical path toward the joint area and the lower frame. This mechanism is effective in reducing stress accumulation under certain conditions, but it still leaves a weakness regarding global bending between the plate panels.

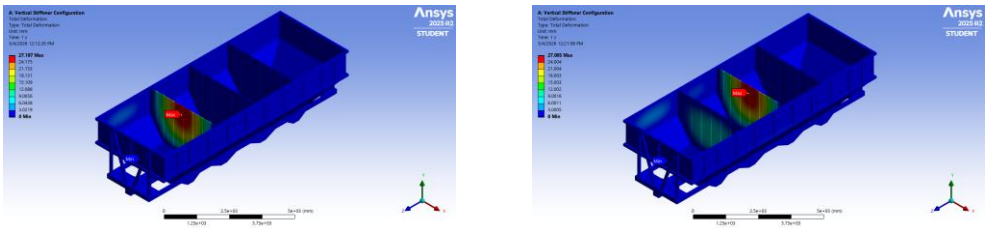

(a) 1 (b) 1-2

(c) 1-2-3 (d) 1-2-3-4

Fig. 8 Total deformation simulation on vertical stiffener configuration

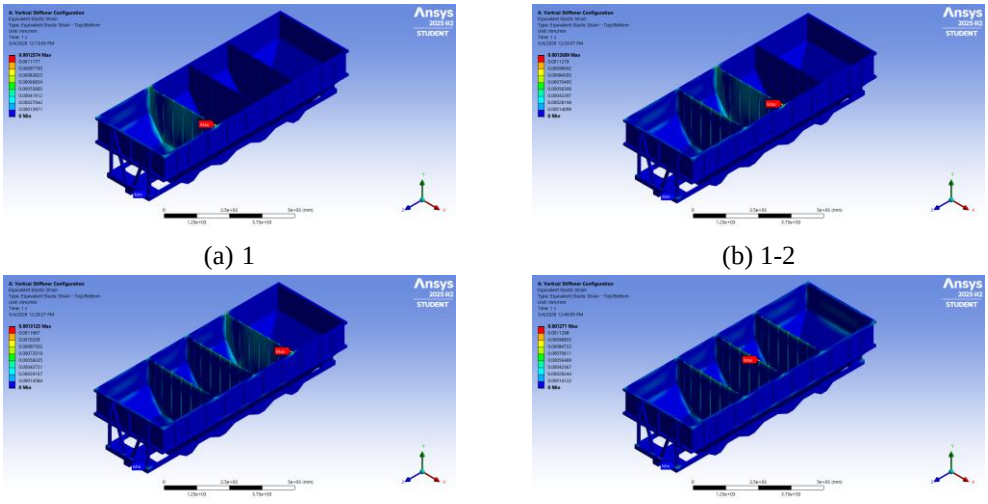

(a) 1 (b) 1-2

(c) 1-2-3 (d) 1-2-3-4

Fig. 9 Equivalent elastic strain on vertical stiffener configuration

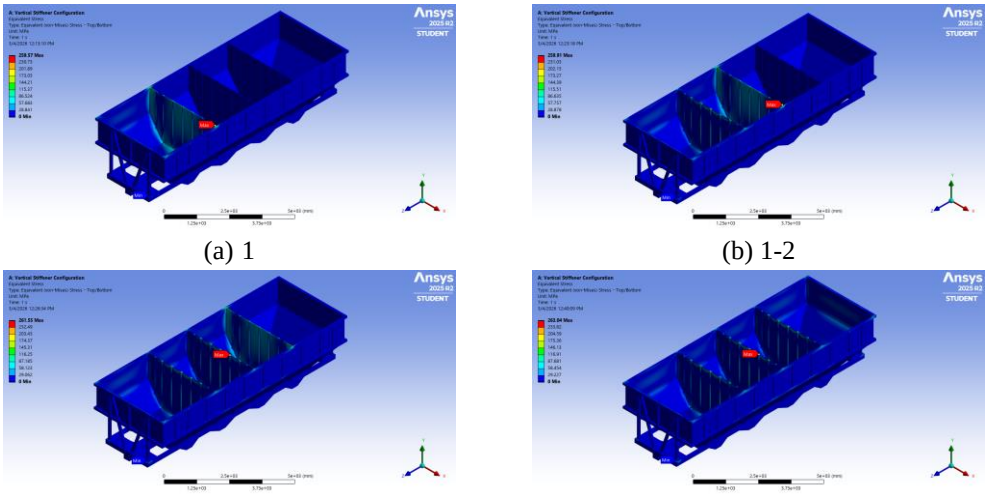

(a) 1 (b) 1-2

(c) 1-2-3 (d) 1-2-3-4

Fig. 10 Equivalent (von-Mises) stress simulation on vertical stiffener configuration

Table 3 Simulation results of vertical stiffener configuration

Loading combination	Total deformation (mm)	Equivalent elastic strain	Equivalent (von-Mises) stress (MPa)
1	27.197	0.0012574	259.57
1 - 2	27.005	0.0012689	259.91
1 - 2 - 3	26.751	0.0013125	261.55
1 - 2 - 3 - 4	8.4865	0.001271	263.04

The maximum deformation occurred at load step 1 (27.197 mm), while the minimum value occurred at load steps 1-2-3-4 (8.4865 mm). The average deformation (δ_{ave}), deformation range ($\Delta\delta$), average equivalent elastic strain (ε_{ave}), equivalent elastic strain range ($\Delta\varepsilon$), theoretical yield strain (ε_y), and strain percentage ($\varepsilon\%$) are calculated using the following equations:

$$\delta_{ave} = \frac{\sum \delta}{n} \tag{2}$$

$$\Delta\delta = \delta_{\max} - \delta_{\min} \tag{3}$$

$$\varepsilon_{ave} = \frac{\sum \varepsilon}{n} \tag{4}$$

$$\Delta\varepsilon = \varepsilon_{\max} - \varepsilon_{\min} \tag{5}$$

$$\varepsilon_y = \frac{\sigma_y}{E} \tag{6}$$

$$\varepsilon\% = \frac{\varepsilon_{\max}}{\varepsilon_y} \tag{7}$$

where $\sum \delta$ is the deformation summation, n is the number of deformations or strains, δ_{max} is the maximum deformation, δ_{min} is the minimum deformation, $\sum \varepsilon$ is the strain summation, ε_{max} is the maximum strain, ε_{min} is the minimum strain, σ_y is the yield stress, E is the Young modulus, and ε_y is the yield strain.

The values of (δ_{ave}) and ($\Delta\delta$) are 22.3599 mm and 18.7105 mm, respectively. The ($\Delta\delta$) fairly wide range indicates that the vertical stiffener configuration is highly sensitive to variations in load distribution. Physically, this suggests that the vertical stiffeners are not yet capable of distributing stiffness evenly across the entire plate.

For the equivalent elastic strain parameter, the maximum value occurs at loading stages 1-2-3, at 0.0013125, while the minimum value occurs at loading stage 1, at 0.0012574. The values of (ε_{max}) and ($\Delta\varepsilon$) are 0.00127745 and 0.0000551, respectively. To evaluate how close the material is to its elastic limit, the values of (ε_y), and ($\varepsilon\%$) are 0.00169048 and 77.63%, respectively. The value of ($\varepsilon\%$) indicates that, despite the significant deformation, the material is still operating within the elastic range with a sufficient safety margin.

For the equivalent von Mises stress parameter, the maximum value occurred under load 1-2-3-4 at 263.04 MPa, while the minimum value occurred under load 1 at 259.57 MPa. The average stress (σ_{ave}), stress range ($\Delta\sigma$), stress percentage ($\sigma\%$), remaining stress percentage ($\sigma_{rem}\%$) and safety factor (SF) can be calculated using the following equations:

$$\sigma_{ave} = \frac{\sum \sigma}{n} \tag{8}$$

$$\Delta\sigma = \sigma_{\max} - \sigma_{\min} \tag{9}$$

$$\sigma\% = \frac{\sigma_{\max}}{\sigma_y} \tag{10}$$

$$\sigma_{rem}\% = 100\% - \sigma\% \tag{11}$$

$$SF = \frac{\sigma_y}{\sigma_{\max}} \tag{12}$$

where $\sum \sigma$ is the stress summation, n is the number of stresses, σ_{max} is the maximum stress, σ_{min} is the minimum stress, and σ_y is the yield stress 9, 10.

The values of (σ_{ave}), ($\Delta\sigma$), ($\sigma\%$), ($\sigma_{rem}\%$) and (SF) are 261.02 MPa, 3.47 MPa, 74.10%, 25.90%, and 1.35, respectively. The very small ($\Delta\sigma$) indicates that the stress distribution in this configuration is relatively uniform across all loading scenarios. Thus, the vertical stiffener configuration can be considered safe in terms of stress, but less effective in controlling the structure's global deformation.

3.2 Structural response of rectangular stiffener configuration

The simulation results for the rectangular stiffener are shown in Figs. 11-13 and Table 4. The same calculation procedure as described in Section 3.1 was applied to determine the average value, range, and utilization ratio for each parameter. In the rectangular stiffener configuration, the grid pattern formed by the combination of vertical and horizontal stiffeners provides increased stiffness to the hopper plate. This is evident from the lower deformation values compared to the vertical configuration. However, this increase in stiffness is accompanied by a significant increase in stress concentration, causing the force distribution to become more concentrated and triggering increased stress in certain areas.

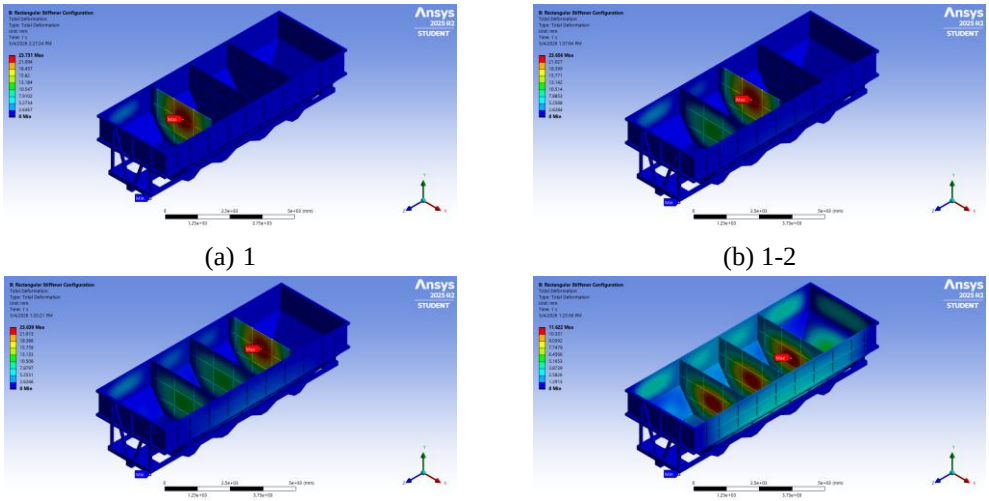

(a) 1 (b) 1-2

(c) 1-2-3 (d) 1-2-3-4

Fig. 11 Total deformation simulation on rectangular stiffener configuration

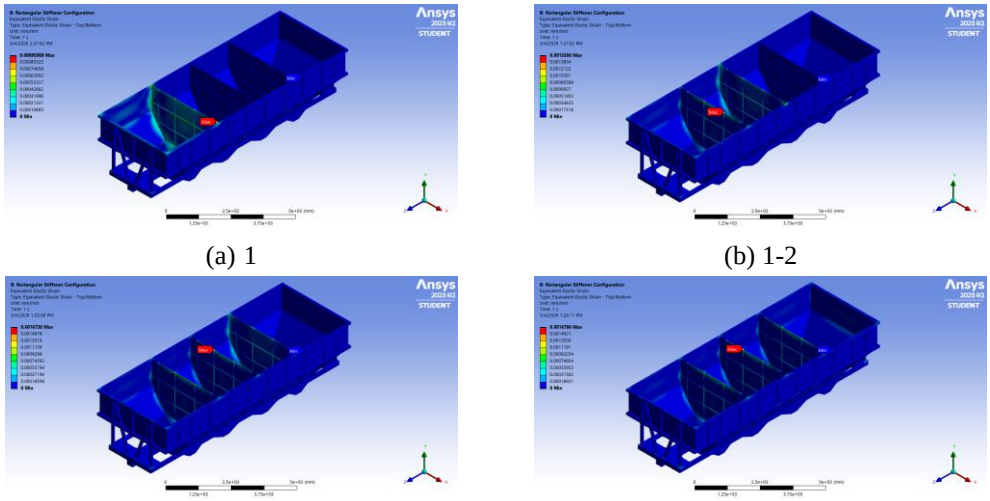

(a) 1 (b) 1-2

(c) 1-2-3 (d) 1-2-3-4

Fig. 12 Equivalent elastic strain on rectangular stiffener configuration

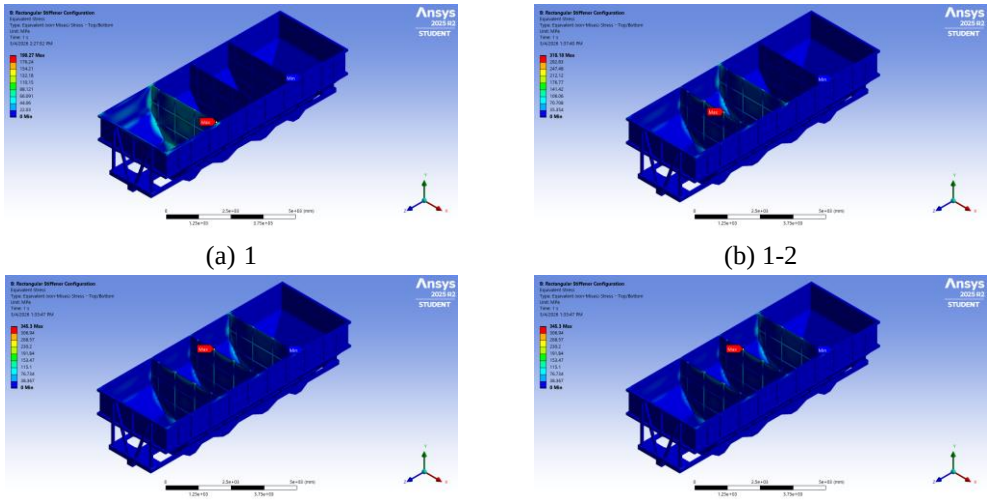

(a) 1 (b) 1-2

(c) 1-2-3 (d) 1-2-3-4

Fig. 13 Equivalent (von-Mises) stress simulation on rectangular stiffener configuration

Table 4 Simulation results of rectangular stiffener configuration

Loading combination	Total deformation (mm)	Equivalent elastic strain	Equivalent (von-Mises) stress (MPa)
1	23.731	0.00095989	198.27
1 - 2	23.656	0.0015586	318.18
1 - 2 - 3	23.639	0.0016738	345.30
1 - 2 - 3 - 4	11.622	0.0016786	346.31

The maximum deformation value occurred at load level 1, at 23.731 mm. The minimum value occurred at load levels 1-2-3-4, at 11.622 mm. The values of (δ_{ave}) and $(\Delta\delta)$ are 20.662 mm and 12.109 mm, respectively. Compared to the vertical configuration, this configuration is more effective in reducing deformation. Rectangular stiffeners also provide a more stable response to variations in loading. However, these effects require further analysis using strain and stress parameters.

For the equivalent elastic strain parameter, the maximum value occurred at loading stages 1-2-3-4, at 0.0016786, while the minimum value occurred at loading stage 1, at 0.00095989. The values of (ε_{ave}), $(\Delta\varepsilon)$, and $(\varepsilon\%)$ are 0.0014677, 0.0007187, and 99.30%, respectively. The $(\varepsilon\%)$ value indicates that the maximum strain in the rectangular configuration is nearly at the material's elastic yield point. This condition suggests that, despite smaller deformations, the stress distribution within the structure tends to become more concentrated. As a result, certain areas are likely to experience critical conditions.

For the equivalent von Mises stress parameter, the maximum value occurred under load 1-2-3-4 at 346.31 MPa, while the minimum value occurred under load 1 at 198.27 MPa. The values of (σ_{avg}), $(\Delta\sigma)$, $(\sigma\%)$, $(\sigma_{rem}\%)$, and (SF) are 302.52 MPa, 148.04 MPa, 97.55%, 2.45%, and 1.03, respectively. This value indicates that the rectangular configuration approaches the material's yield point. With the low safety factor, this configuration poses a high risk if applied to real-world operational conditions involving load variations and structural imperfections.

3.3 Structural response of triangulated stiffener configuration

The simulation results for the triangulated stiffener are shown in Figs. 14-16 and Table 5. Among the three designs analyzed, the triangulated stiffener configuration exhibits the most balanced response. The same calculation procedure as described in Section 3.1 was applied to determine the average value, range, and utilization ratio for each parameter.

The triangulation pattern creates a more direct force distribution path. This causes the load from granular pressure to be borne not only through plate bending. The load is also transferred through tensile and compressive mechanisms in the stiffening elements. This characteristic makes the structure globally stiffer and more stable, therefore enhancing structural performance under changing load distributions.

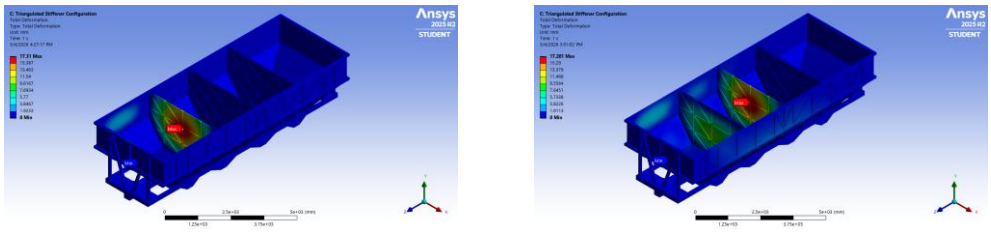

(a) 1 (b) 1-2

(c) 1-2-3 (d) 1-2-3-4

Fig. 14 Total deformation simulation on triangulated stiffener configuration

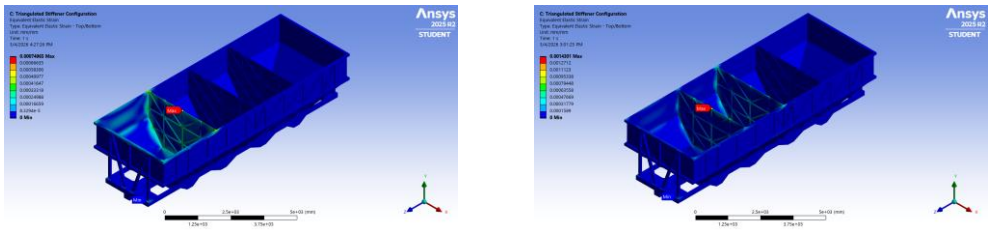

(a) 1 (b) 1-2

(c) 1-2-3 (d) 1-2-3-4

Fig. 15 Equivalent elastic strain on triangulated stiffener configuration

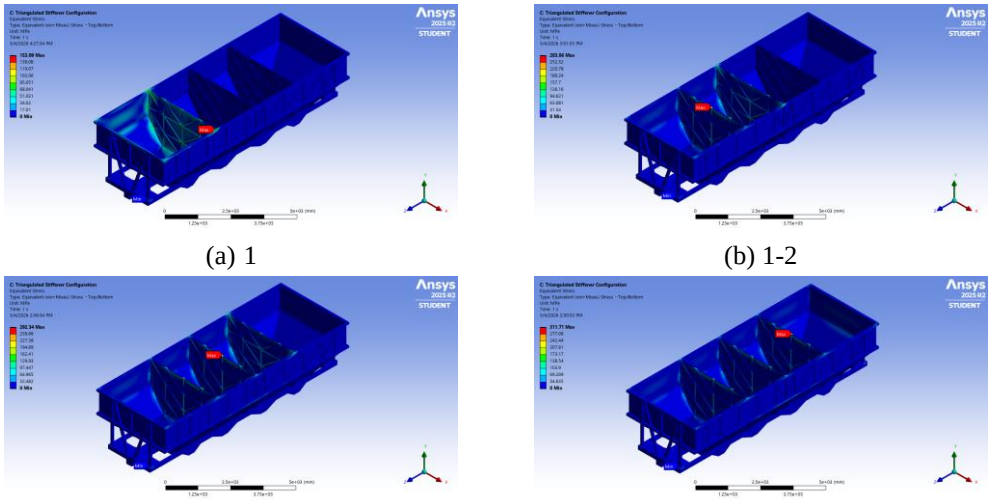

(a) 1 (b) 1-2

(c) 1-2-3 (d) 1-2-3-4

Fig. 16 Equivalent (von-Mises) stress simulation on triangulated stiffener configuration

Table 5 Simulation results of triangulated stiffener configuration

Loading combination	Total deformation (mm)	Equivalent elastic strain	Equivalent (von-Mises) stress (MPa)
1	17.31	0.00074965	153.09
1 - 2	17.201	0.0014301	283.86
1 - 2 - 3	17.306	0.0014309	292.34
1 - 2 - 3 - 4	10.048	0.0015114	311.71

For the deformation parameters, the maximum value occurred under load 1 at 17.31 mm. The minimum value occurred under loads 1-2-3-4 at 10.048 mm. The values of (δ_{ave}) and ($\Delta\delta$) are 15.466 mm and 7.262 mm, respectively. The (δ_{ave}) value is the lowest among all configurations, and the deformation range is also the smallest. This indicates that the triangulated stiffener has the highest overall stiffness. In addition, this configuration also exhibits the most stable response to variations in load distribution.

For the equivalent elastic strain parameter, the maximum value occurs at loading stages 1-2-3-4, at 0.0015114. The minimum value occurs at loading stage 1, at 0.00074965. The values of (ε_{ave}), ($\Delta\varepsilon$), and (ε%) are 0.0012805, 0.00076175, and 89.41%, respectively. The (ε%) value indicates that the structure remains within an elastic state, although it is higher than that of the vertical configuration.

For the equivalent von Mises stress parameter, the maximum value occurred under load 1-2-3-4 at 311.71 MPa. The minimum value occurred under load 1 at 153.09 MPa. The values of (σ_{avg}), ($\Delta\sigma$), (σ%), (σ_{rem}%), and (SF) are 260.25 MPa, 158.62 MPa, 87.81%, 12.19%, and 1.14, respectively. Although the maximum stress is higher than that of the vertical stiffener, the lower average stress and strain values indicate that the force distribution in this configuration is more efficient. Thus, the triangulated stiffener provides the best balance between stiffness, stability, and structural safety.

4. Discussion

This section discusses the structural behavior of each stiffener configuration based on the finite element simulation results. The discussion focuses on deformation, strain, and stress distribution under different loading conditions. The influence of stiffener topology on structural stability is also evaluated. In addition, the force transfer mechanism of each configuration is analyzed to identify the most effective reinforcement design for hopper wagon structures.

4.1 Comparative structural performance

A comparison of the configurations shows that changes in the stiffener topology directly alter the force distribution mechanism and structural response of the hopper wagon. Based on the calculation results, the triangulated stiffener

configuration produces the lowest average deformation, namely 15.466 mm, while the vertical stiffener configuration has the highest average deformation of 22.3599 mm.

The reduction percentage in average deformation (δ_{ave}) from the triangulated to the vertical configuration is 30.83%. Compared to the rectangular configuration, the reduction percentage in (δ_{ave}) for the triangulated configuration is 25.14%. These results indicate that the triangulated configuration provides the greatest improvement in global stiffness. Physically, this behavior is due to the triangulation mechanism, which allows forces to be transmitted through more efficient tension-compression paths, thereby reducing deformation caused by plate bending.

In terms of average stress (σ_{ave}), the triangulated configuration also demonstrates better performance, with a value of 260.25 MPa, compared to 261.02 MPa for the vertical stiffener and 302.52 MPa for the rectangular stiffener. The decrease percentage in (σ_{ave}) for the triangulated configuration relative to the vertical one is relatively small (0.29%). However, for rectangular shapes, the reduction reaches 13.97%. This indicates that the rectangular configuration results in a more uneven stress distribution, thereby increasing the overall average stress.

When compared in terms of maximum stress (σ_{max}), the vertical stiffener configuration yields the lowest value, at 263.04 MPa. In contrast, the rectangular stiffener produces the highest (σ_{max}) of 346.31 MPa, corresponding to an increase of 18.50% compared to the vertical configuration. These results show that the vertical configuration remains superior in keeping the maximum stress low. However, this advantage comes at the cost of high global deformation.

The rectangular configuration reduces deformation but results in stresses that approach the material's yield strength. On the other hand, the triangulated configuration exhibits an intermediate maximum stress level but provides a more balanced overall deformation and stress distribution. A summary of the derived structural response parameters for the three configurations is presented in Tables 6-7.

Table 6 Summary of derived structural response parameters, part 1

Configuration	Average deformation (mm)	Deformation range (mm)	Average strain	Maximum strain utilization (%)
Vertical	22.3599	18.7105	0.00127745	77.63
Rectangular	20.6620	12.1090	0.0014677	99.30
Triangulated	15.4660	7.2620	0.0012805	89.41

Table 7 Summary of derived structural response parameters, part 2

Configuration	Average stress (MPa)	Maximum stress (MPa)	Stress utilization (%)	Safety factor
Vertical	261.02	263.04	74.10	1.35
Rectangular	302.52	346.31	97.55	1.03
Triangulated	260.25	311.71	87.81	1.14

4.2 Critical loading combinations analysis

The load scenario analysis shows that critical conditions are not always identical for every observed parameter. In the vertical stiffener configuration, maximum deformation occurs under loading 1, while maximum stress occurs under loadings 1-2-3-4. This indicates that localized loading in a single compartment can trigger significant global bending. In contrast, full loading increases stress accumulation due to the even distribution of pressure across the entire hopper wall.

In the rectangular stiffener configuration, the 1-2-3-4 loading case is the most critical condition for both strain and stress. The increased stiffness resulting from the grid pattern causes the forces to be concentrated at the intersections of the stiffening elements. Consequently, under full loading conditions, the maximum stress increases significantly and approaches the material's yield strength.

In the triangulated stiffener configuration, maximum deformation still occurs under loading condition 1, while maximum strain and stress occur under loading conditions 1-2-3-4. This indicates that although the structure achieves improved overall stability, asymmetric load distribution can still result in relatively high deformation under certain conditions. However, the overall structural response remains more controlled compared to other configurations.

These findings confirm that a multi-compartment loading approach is essential in the analysis of hopper wagons. Uniform loading alone is insufficient to represent actual operating conditions, as the most critical structural responses may arise from uneven load distributions.

4.3 Structural mechanics interpretation and design implications

The performance of each stiffener configuration is significantly influenced by the force distribution paths formed within the structure. In the vertical stiffener configuration, forces induced by granular pressure are predominantly transmitted along the direction of the vertical stiffeners. This results in relatively low maximum stresses of 263.04 MPa. However, because there are no stiffeners in the transverse direction, the hopper plate still experiences significant bending, resulting in the highest average deformation of 22.3599 mm among all configurations. In this configuration, nine vertical stiffeners were distributed along the hopper wall with an average spacing of approximately 1.1 m. The relatively large unsupported plate regions between stiffeners still allow considerable global bending deformation to occur. In general, deformation tends to increase as the spacing between adjacent stiffeners becomes larger, as expressed in the following relationship:

$$\delta \propto s \tag{13}$$

where δ represents deformation and s represents the spacing between adjacent stiffeners.

In the rectangular stiffener configuration, the presence of horizontal elements increases the panel's stiffness and reduces deformation. The average deformation decreased to 20.662 mm due to the reduced effective plate span between stiffeners. However, the interaction between vertical and horizontal members creates stiff zones at the intersection points. These zones act as stress concentration points, particularly under full loading conditions. As a result, the rectangular configuration produces the highest maximum stress of 346.31 MPa, with a safety factor of only 1.03. Smaller rectangular grid spacing may further reduce plate deformation. Nevertheless, excessive grid density may increase stress concentration near welded intersections and connection regions.

Conversely, the triangulated stiffener configuration operates based on the principle of triangular geometric stability. Forces are not only resisted through bending but also distributed through tensile and compressive mechanisms between elements. The diagonal members introduce additional load transfer paths, making the plate bending effect less dominant compared to the other configurations. This configuration produced the lowest average deformation of 15.466 mm while maintaining an average stress of 260.25 MPa. Although the maximum stress reached 311.71 MPa, the overall deformation and stress distribution remained more stable under different loading conditions. In general, increasing the number of effective stiffening members tends to improve wall stiffness and reduce deformation, as expressed below:

$$\delta \propto \frac{1}{n} \tag{14}$$

where n is the number of stiffeners contributing to load transfer.

Overall, these results demonstrate that the triangulation-based topology holds strong potential for enhancing the structural efficiency of hopper wagons. This configuration not only increases stiffness but also keeps the stress distribution within safe limits under various loading conditions. The present findings also indicate that stiffener spacing, panel dimensions, and reinforcement topology should be considered simultaneously during hopper wall design. Smaller panel dimensions generally improve stiffness performance; however, this must be balanced against increased fabrication complexity, welding length, structural weight, and manufacturing cost.

5. Conclusions

This study investigated the influence of stiffener configurations on the structural behavior of hopper wagons using a finite element approach under a multi-compartment loading scenario. The analysis was conducted on three main configurations—

vertical, rectangular, and triangulated stiffeners—while accounting for the non-uniform distribution of granular material pressure to represent more realistic operational conditions. This approach enables the identification of structural responses under more complex loading conditions than those associated with uniform distributions. Additionally, this analysis reveals how stiffener topology affects force distribution within the hopper structure. The main conclusions obtained are as follows:

(1) The structural response of the hopper wagon is strongly influenced by the stiffener topology. Different reinforcement layouts modify the force transfer mechanism and stiffness distribution, resulting in distinct deformation and stress characteristics.

(2) The vertical stiffener configuration provides a favorable safety margin with relatively low stress levels. However, its effectiveness in controlling global deformation remains limited due to the absence of transverse reinforcement.

(3) The rectangular stiffener configuration enhances structural rigidity by reducing plate deformation. Nevertheless, the interaction between vertical and horizontal members tends to create localized stress concentrations, which may reduce structural reliability under varying loading conditions.

(4) The triangulated stiffener configuration promotes a more efficient load transfer mechanism through tensile and compressive force paths. This characteristic contributes to a more balanced structural response in terms of stiffness, deformation control, and stress distribution.

(5) The multi-compartment loading approach demonstrates that critical structural conditions do not necessarily occur under fully loaded conditions. Therefore, non-uniform loading scenarios should be considered to better represent the actual operating conditions of hopper wagons.

(6) Overall, the triangulated stiffener configuration exhibits the most balanced structural performance among the configurations evaluated. This approach offers significant potential for improving stiffness, stability, and structural efficiency.

(7) Future research should focus on optimizing stiffener spacing, quantity, and geometric dimensions to further improve structural efficiency. The effects of dynamic loading, fatigue behavior, material nonlinearity, and experimental validation should also be investigated. These aspects are expected to provide a more comprehensive understanding of hopper wagon structural performance under real service conditions.

Conflicts of Interest

The authors declare no conflict of interest.

References

[1] H. Huang, Y. Zhang, D. Wang, Z. Fu, H. Tian, J. Shang, et al., “Study the Flow Capacity of Cylindrical Pellets in Hopper with Unloading Paddle Using DEM,” Agriculture, vol. 14, no. 4, article no. 523, 2024.

[2] P. Chen, T. Huang, B. Wu, H. Qian, F. Xie, B. Liu, et al., “Modeling the Discharge Rate of a Screw Conveyor Considering Hopper–Conveyor Coupling Parameters,” Agriculture, vol. 14, no. 7, article no. 1203, 2024.

[3] X. Bi, N. Zhao, M. Guo, W. Zhang, F. Zhou, W. Xie, et al., “Synergistic Redox and Adsorption for Enhanced Roxarsone Removal: Heterogeneous Fenton-Like Reaction with a Novel Composite of Nanoscale Zero-Valent Iron Supported on γ-Aluminum Oxide,” Chemical Engineering Science, vol. 287, no. 5, article no. 119713, 2024.

[4] N. Nikolopoulos, E. Kordouli, L. Sygellou, K. Bourikas, C. Kordulis, and A. Lycourghiotis, “Mo Promoted Ni-ZrO_2 CO-Precipitated Catalysts for Green Diesel Production,” Chemical Engineering Science, vol. 270, no. 3, article no. 118540, 2023.

[5] Y. Zhou, T. Wang, and J. Zhu, “Development of Gas-Solid Fluidization: Particulate and Aggregative,” Powder Technology, vol. 421, article no. 118420, 2023.

[6] Y. Deng, H. Jiang, and Y. Ren, “Low-Velocity Impact Resistance Behaviors of Bionic Double-Helicoidal Composite Laminates,” International Journal of Mechanical Sciences, vol. 248, article no. 108248, 2023.

[7] Y. Ichiyanagi, Y. Michitsuji, A. Matsumoto, Y. Sato, H. Ohno, S. Ogata, et al., “Simulation-Based Estimation of Wheel/Rail Friction Coefficient and Wear Number Considering Results of Full-Scale Roller-Rig Test,” Mechanical Engineering Journal, vol. 10, no. 3, pp. 1-11, 2023.

[8] Q. Ye, Q. Luo, G. Feng, T. Wang, and H. Xie, "Stress Distribution in Roadbeds of Slab Tracks with Longitudinal Discontinuities," Railway Engineering Science, vol. 31, no. 1, pp. 61-74, 2023.

[9] J. D. Pozo, M. A. Hube, and Y. C. Kurama, "Quantification of Variability in Simulated Seismic Performance of RC Wall Buildings," Engineering Structures, vol. 295, article no. 116872, 2023.

[10] Z. Li, J. Fan, J. Xu, G. Feng, W. Guo, J. Cui, et al., "Experimental and Simulation Research on Rupture Behavior of Coal-Based Solid Waste Material Backfilling Column under Non-uniformly Distributed Load with Different Loading Ratios," Case Studies in Construction Materials, vol. 20, no. 7, article no. e03125, 2024.

[11] I. V. Kotov, R. Yu. Litvinov, A. V. Nefedov, and O. N. Chicheneva, "Vibrating Device for the Collapse of Bulk Materials in the Hoppers of the Sintering Shop," CIS Iron and Steel Review, vol. 29, pp. 33-36, 2025.

[12] D. E, B. Zhao, J. Cui, Z. Zhou, W. Sun, Y. Qiu, et al., "DEM Study on the Optimization of Asymmetric Hopper Configurations," Powder Technology, vol. 473, article no. 122224, 2026.

[13] Y. Song, Q. Lin, and J. Chen, "Research Progress on Curved Plates in China: Mechanical Analysis Methods and Load-Bearing Behaviours," Structures, vol. 39, pp. 793-807, 2022.

[14] E. Sabbioni, M. Carboni, D. Tarsitano, and S. Bruni, "Crack Detection in Railway Axles Using Continuous Monitoring and Periodic Non-destructive Inspection: Experimental Investigation on a Freight Wagon Using a Full-Scale Roller Rig," Structural Health Monitoring, vol. 24, no. 6, pp. 3487-3502, 2025.

[15] J. Lv, "Analysis of Dynamic Response Characteristics of Vehicle-Mounted Tank based on the Finite Element Method," Journal of Vibroengineering, vol. 28, no. 1, pp. 143-159, 2026.

[16] Q. Xiao, M. Zhang, D. Chen, X. Wang, and C. Lei, "The Operational Performance and Fatigue Life Analysis of Internal Suspension Bogie," Journal of the Brazilian Society of Mechanical Sciences and Engineering, vol. 47, no. 12, article no. 634, 2025.

[17] P. W. Cleary and M. L. Sawley, "DEM Modelling of Industrial Granular Flows: 3D Case Studies and the Effect of Particle Shape on Hopper Discharge," Applied Mathematical Modelling, vol. 26, no. 2, pp. 89-111, 2002.

[18] G. Dyck, A. Rogers, and J. Paliwal, "A Review of Analytical Methods for Calculating Static Pressures in Bulk Solids Storage Structures," KONA Powder and Particle Journal, vol. 41, pp. 108-122, 2024.

[19] E. Eidin, T. Bielik, I. Touitou, J. Bowers, C. McIntyre, D. Damelin, et al., "Thinking in Terms of Change Over Time: Opportunities and Challenges of Using System Dynamics Models," Journal of Science Education and Technology, vol. 33, no. 1, pp. 1-28, 2024.

[20] G. Vatulia, J. Gerlici, O. Fomin, A. Lovska, Y. Fomina, and K. Kravchenko, "Analysis of the Strength of the Supporting Structure of a TwoSection Hopper Wagon under Operating Loading Conditions," Applied Sciences, vol. 13, no. 2, article no. 859, 2023.

[21] S. Panchenko, J. Gerlici, A. Lovska, V. Ravlyuk, J. Dižo, and J. Harušinec, "Study on the Strength of the Brake Pad of a Freight Wagon under Uneven Loading in Operation," Sensors, vol. 24, no. 2, article no. 463, 2024.

[22] K. Sookchanchai, S. Joonjitdumrong, and V. Uthaisangsuk, "Structural Assessment of Flat Waggon Underframe for Freight Rail by Experiments and FE Analyses," Australian Journal of Mechanical Engineering, vol. 24, no. 1, pp. 127-156, 2026.

[23] A. Scherbakov, M. Aleksandrovskiy, D. Shavelkin, and N. Verbova, "Method for Obtaining Structures with a Given Degree of Dispersion in Low-Carbon and Low-Alloy Steels of Transport and Handling Equipment," in Networked Control Systems for Connected and Automated Vehicles, Cham: Springer, pp. 1253-1264, 2023.

[24] A. Teter and Z. Kolakowski, "Interactive Buckling of Wide Plates Made of Functionally Graded Materials with Rectangular Stiffeners," Thin-Walled Structures, vol. 171, article no. 108750, 2022.

[25] C. Chen, S. Li, J. Li, L. Zhang, and J. Yang, "Influence of Ballast Gradation on Repose Angle Using Large-Scale Hopper Flow Tests and DEM Simulation," Powder Technology, vol. 456, article no. 120852, 2025.

[26] S. Zhang, G. Yang, and X. Zhang, "Effect of Boundaries on Flow Behavior of Granular Material in a Hopper," Powder Technology, vol. 466, article no. 121505, 2025.

[27] U. Ulusoy, "A Review of Particle Shape Effects on Material Properties for Various Engineering Applications: From Macro to Nanoscale," Minerals, vol. 13, no. 1, article no. 91, 2023.